UNIVERSITY OF CALIFORNIA
RIVERSIDE

Synthetic Aperture Technology Applied to OCT and an Analysis of Neuronal Swelling

A Thesis submitted in partial satisfaction
of the requirements for the degree of

Master of Science

in

Bioengineering

by

Christopher Lee Hughes

June 2016

Thesis committee:

Dr. Hyle Park, Chairperson
Dr. Victor Rodgers
Dr. William Grover

The Thesis of Christopher Lee Hughes is approved:

_____

_____

_____

Committee Chairperson

University Of California, Riverside

Table of Contents

List of Figures

Chapter 1

Chapter 2

Introduction

In the NOIR Lab at UCR, our goal is to apply optics to the study of the nervous system. The currently available technology that is best suited for this task is Optical Coherence Tomography (OCT) because of its ability to penetrate tissue and create depth-resolved images in a label free manner. Furthermore, using changes in optical scattering that occur during activity, OCT is able to detect neural activity. OCT is able to obtain a lateral resolution on the order of microns, which is needed to image neurons. The ability of OCT to resolve images of this size is determined by the wavelength of the laser source and the numerical aperture. A larger numerical aperture results in a higher resolution but also leads to a smaller depth of focus. It is of interest to maintain a high resolution and also increase our depth of focus. In order to do this, I propose to implement synthetic aperture technology, which has been previously demonstrated to work in an OCT system.[1,2] Though it has previously been demonstrated that synthetic aperture can be used to increase the intensity, or SNR, of images, the effect on phase has not been studied. Since we use phase measurements for the detection of activity, it is of interest to us to see what effect this technology may have on the phase in addition to the intensity.

In this project, I will apply synthetic aperture technology to our OCT system to improve the depth of focus and analyze the effects on phase.

Background

Optical Coherence Tomography (OCT) is an optical method that uses light scattering to form 3D images.[3] OCT is based on low-coherence interferometry which means light from two sources, the sample arm and reference arm, are superimposed to extract information about the waves, such as phase and amplitude, which is important for resolving

3D images. OCT is useful because it is non-invasive, doesn't require labels, and is able to penetrate more deeply into tissue than other optical methods, such as confocal microscopy. OCT is typically used in biological applications including ophthalmology, cardiology, and, more progressively, neuroscience.

The sample arm of an OCT apparatus is where the tissue of interest is located. The reference arm contains a source of reference, typically a mirror, which reflects light back and gives us a basis for our measurements. After being reflected from these two arms, the light is then recombined (interferometry) and diverted to a recording device by a beam splitter. The data is stored as complex arrays in a computer to be processed later.

In the sample arm, there is a mechanism that scans light over the tissue of interest. Each time light is directed at tissue, a line is obtained which corresponds to the point of light and its total depth of penetration; this is called an A-line. A series of these A-lines can form 2D images that correspond to the scanned plane; this is called a B-line. A series of B-lines can then be combined to form a 3D image of the scanned tissue.

Historically, the first type of OCT was Time Domain OCT (TD-OCT). This method involves the movement of the reference mirror. By moving the mirror, the interference patterns received then will correspond to a depth of the sample corresponding to the distance the mirror has been moved. This method, though straightforward, has limitations in data collection and image quality due to the relatively long amount of time needed to move the mirror.[4]

After this method, two other techniques took precedence: Spectral Domain OCT (SD-OCT)[5] and Swept-Source OCT (SS-OCT).[6] SD-OCT involves the implementation of a broadband light source. A broadband light source possesses a range of wavelengths with a

central wavelength surrounded by a spectrum of others. The drop off of the intensity of these wavelengths can be characterized by a Gaussian function. Upon return from the sample, the interference pattern is broken up into its components by a grating. By applying a Fourier transform to the data, we can extract the component frequencies from the spectral information. The frequency patterns correspond to the depth of penetration and this information, then, can be used to code for depth.

Swept-source OCT works similarly but, rather than sending a broadband wave in and breaking it up into components, SS-OCT applies narrow-band beams sequentially to a sample. SS-OCT can potentially provide many advantages including increased imaging speed and better resolution.

The systems we currently use are SD-OCT systems. We have an 800 nm system and a 1310 nm system which allows us to image systems at different numerical apertures (discussed later). A schematic of our 800nm system is given below (Figure 1).

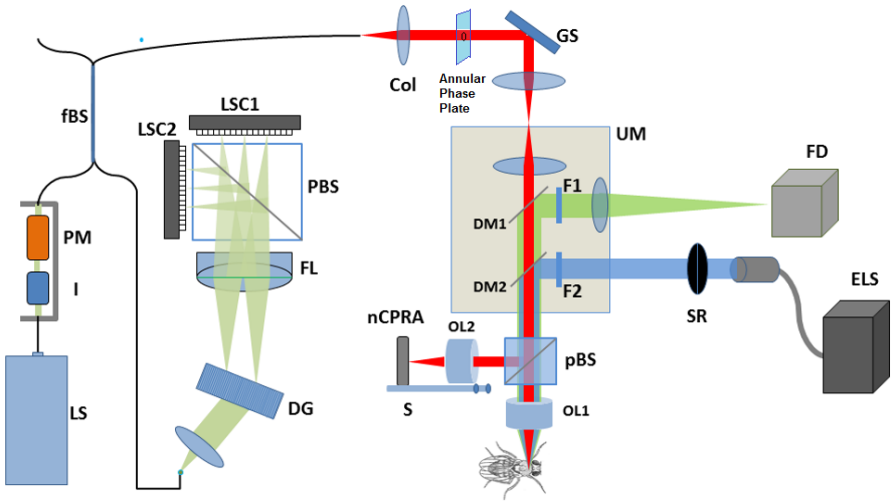

Figure 1: Schematic of 800nm SD-OCT system with implemented synthetic aperture.

One trade-off for the increased depth of imaging in OCT is a decrease in resolution. This can be a problem particularly in neuroscience applications when the detectable changes are on the order of nanometers. In order to increase the capabilities of our system and the effectiveness of our research it is, therefore, paramount that we increase the resolution across a larger depth. An intuitive understanding of this can be derived when we consider the Rayleigh range.[6] The Rayleigh range is the depth across which we consider the resolution useable and is defined as $\sqrt{2}w_0$ where w_0 is the beam waist. A smaller beam waist corresponds to a better resolution (Figure 2).

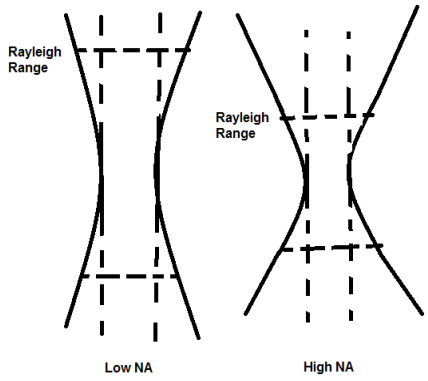

Figure 2: Image demonstrating the difference between a Low NA and High NA. A higher NA decreases the size of the beam waist, but also a decrease in the Rayleigh Range.

This relationship can be further explained in terms of numerical aperture.[7,8] Numerical aperture (NA) is a dimensionless number that characterizes the range of angles over which the system can accept or emit light. The equation that describes the NA is given as follows:

$$NA = nsin\theta$$

Where n is the refractive index of the medium of the lens and θ is the measure of the half-angle of the maximum cone of light. The resolution of an imaging system describes its ability to resolve detail. The resolution is directly proportional to NA and its equation is given as

$$r = \frac{1.22\lambda}{2NA} = \frac{0.61\lambda}{NA}$$

Where r is the minimum distance between distinguishable points and λ is the wavelength of the light. Therefore, when NA is higher, the minimum distance between distinguishable points is lower which means the resolution is higher. The depth of field (DOF) is the range near and far objects can be considered effectively focused. DOF is inversely proportional to NA and its equation is given as follows:

$$DOF = \frac{\lambda n}{NA^2}$$

The DOF, then, is inversely proportional to NA. Therefore, there exists a trade-off between better resolution and DOF; a high NA lens will provide a better resolution over a smaller depth.

Synthetic Aperture technology is an optical manipulation used to extend the limits of an aperture beyond its normal limits. Synthetic aperture has been most popularly applied in satellite systems.[10] In these systems, a satellite uses radar to record images of the Earth. The movement of the satellite is used as a scanning mechanism to obtain an image larger than what would be recorded otherwise by the small aperture. The technology works by taking many separate images equivalent to the size of the aperture and then recombining these images based on the reception time and the known Doppler effects into a continuous image that could usually only be obtained with a larger aperture.

From this technology, we can apply further a principle known as aperture synthesis. Aperture synthesis involves an overlap in recorded images. By extracting the best information from each image corresponding to a particular area, we can form a new image with better overall resolution.

The same principles discussed in the context of satellites can be used in optical applications. Previously, a method was demonstrated that relied completely on optical theory to mathematically improve upon the resolution.[11] This method, however, as may be gleaned from the description, was computationally intensive. A simpler and elegant way that has more recently been demonstrated involves the use of an annular glass plate to create a change in the optical path length of the light.[1]

A simple and intuitive way of describing this technology is in terms of the wavefronts (Figure 3). Objects that are in focus correspond to a flat wavefront when passing through the lens. Anything outside of the focus has a curved wavefront when passing through the lens. The more curved the wavefront, the poorer the resolution of the image will be. Using the annular phase plate, we can break up the wave into multiple segments where the inner segments, for a fair distance, can be approximated as being flat. The outer images we can correct by a factor dz which corresponds to how much the wave is curved. This allows us to process the wavefront into a flatter form which will increase the resolution.

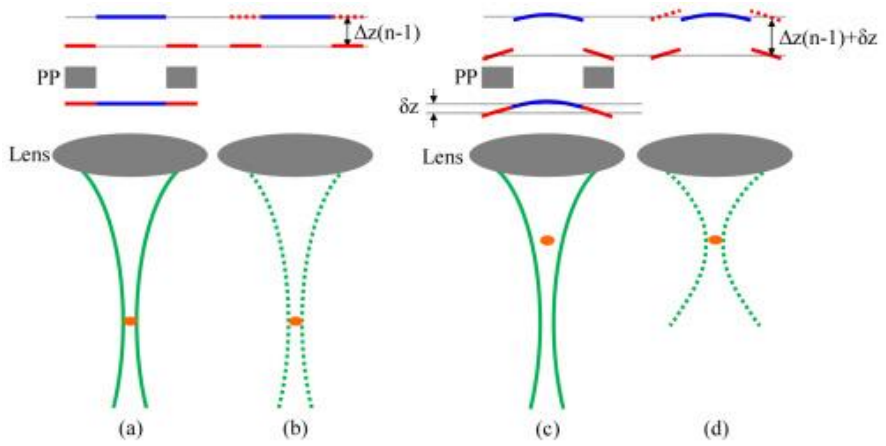

Figure 3: (From de Boer paper) Image showing intuitive description of resolution improvement with synthetic aperture. A) A beam front from in focus being separated into two images of different depth by the annular phase plate. B) Correction of the change in path length caused by the phase plate in image A. C) A beam front from out of focus being separated into two images of different depth by the annular phase plate. D) Correction of the change in path length caused by the phase plate in image C and correction for the small extra delay dz caused by the image being out of focus.

Experimental Design

In order to test if this technology can be applied to our system, we first create a glass plate with parameters based on the following calculations. Rather than ordering custom glass immediately, we first focus on creating a glass plate using a glass slide of known thickness to ensure the theory matches the measurements. We will later want to order custom glass to optimize the depth of focus for our system. The first step in this process is calculating the diameter of the hole needed which is based on the thickness of the beam of light and its Gaussian profile. We want to use this information to create a hole that lets through 50% of the total intensity of light while the rest goes through the glass. Once we have designed this set-up, we need to write code that can split up the three distinct images and then recombine them into an image with an increased resolution through phase manipulations. Theoretically this should be dependent on the thickness and index of refraction of the glass, but we will

design an algorithm that optimizes the parameters through iterative methods. If the system works correctly, we expect to see an increased lateral resolution over a larger depth of focus.

The annular phase plate is created from a normal glass plate of a specific thickness by inserting a hole in the center of the plate (Figure 4).

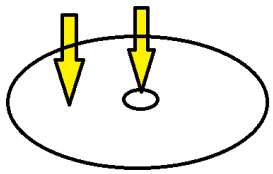

Figure 4: A schematic of the annular phase plate. The arrows represent the different possible paths of light, through the glass and through the hole.

This hole must be of a specific size which corresponds to the beam diameter and its Gaussian profile. The ideal size for the hole can be derived from properties of a Gaussian beam. Ideally, we want an equal amount of light moving through the hole as we have moving through the glass, as mentioned previously. If we imagine the hole and surrounding lens as a circle, the intensity across an area can be expressed as the integral of the intensity function multiplied by the circumference of a circle relative to the radius. To ensure we have an equal amount of intensity moving through the hole and the glass, we integrate from the center to the edge of the hole (the diameter) and set this equal to the integral of the edge of the hole to the end of the beam. This equation is given as

$$\int_0^d 2\pi r * I(r) = \int_d^w 2\pi r * I(r) \quad (1)$$

Where *r* is the radius, *d* is the diameter of the hole, *w* is the width of the beam, and *I(r)* is the intensity as a function of radius. For a Gaussian beam, the intensity function can be described with the following equation:

$$I(r) = I_0 e^{-\frac{r^2}{w^2}} \ (2)$$

Where I_0 is the intensity at the peak, r is the full radius of the beam, w is the radius at which the intensity of the beam drops to 1/e of its initial value. We can solve for w by setting the above equation equal to I_0 multiplied by a factor of $1/e^2$. The full radius of the beam is constant for a given wavelength and can be found from the THORlabs website for a given beam.

Using equations 1 and 2, we can solve for the ideal diameters for each wavelength

800nm

$$\frac{1}{e^2} I_0 = I_0 e^{-\frac{.5^2}{w^2}}$$

$$w = \ 0.3535$$

$$\int_0^d 2\pi r * e^{-\frac{r^2}{.125}} = \int_d^{8mm} 2\pi r * e^{-\frac{r^2}{.125}}$$

$$-0.0625e^{-8d^2} + 0.0625 = -0.0625e^{-8*8^2} + 0\,.0625e^{-8d^2}$$

$$0.125e^{-8d^2} = 0.0625$$

$$-8d^2 = -0.69$$

$$\underline{\boldsymbol{d = 0.29}}$$

1300nm

$$\frac{1}{e^2} I_0 = I_0 e^{-\frac{.71^2}{w^2}}$$

$$w = 0.5021$$

$$\int_0^d 2\pi r * e^{-\frac{r^2}{0.252}} = \int_d^{8mm} 2\pi r * e^{-\frac{r^2}{0.252}}$$

$$-0.126e^{-3.96d^2} + 0.126 = -0.126e^{-3.96*8^2} + 0.126e^{-3.96d^2}$$

$$0.25e^{-3.96d^2} = 0.126$$

$$-3.97d^2 = -0.69$$

$$\underline{\boldsymbol{d = 0.42}}$$

The presence of a hole allows the possibility for light to take three different paths: in and out through the hole, in the hole and out through the glass (or vice-versa), or in and out through the glass. Each of these paths will have different optical path lengths (OPLs) based on the index of refraction of the glass and its thickness. The change in path length can be described as

$$\Delta OPL = \Delta z(n-1)$$

Where Δz is the thickness of the glass and n is the index of refraction of the medium. For the light that goes through the hole when traveling towards the sample and when returning, there is no change in the OPL. For light that travels through the hole once and through the glass once, the change in OPL is $\Delta z(n-1)$. For light that travels through glass twice, the change in is $2\Delta z(n-1)$.

Each of these images corresponds to a different depth of focus based on the change in the optical path length. We can then use the known information about phase and reception time to manipulate these three separate images into one image with an increased depth resolution through aperture synthesis.

This aperture synthesis works on the known theory surrounding OCT. The intensity function for an OCT signal is given:

$$I(k) = I_r(k) + I_s(k) + 2\sqrt{I_r(k)I_s(k)}\alpha\cos(2kz)$$

Where k is the wavenumber, $I_r(k)$ represents the intensity from the reference arm, $I_s(k)$ represents the intensity from the sample arm, and a is the square root of the scattering object reflectivity at depth z. As discussed previously, when the annular phase plate is used, the image is split into three images each encoded to a different depth. These new images add new interference terms to the equation based on the change in optical path lengths and so the equation for the interference term from the previous equation becomes the following:

$$I(k) = \sqrt{I_r(k)I_s(k)}\alpha(e^{i2kz} + e^{i2kz+ik(\Delta z(n-1)+dz)} + e^{i2kz+ik2(\Delta z(n-1)+dz)}) + C.C.$$

Where $\Delta z(n-1)$ is the optical path difference based on the thickness and index of refraction of the phase plate, *C.C.* is the complex conjugate, and dz is the curvature of the wavefront, which we aim to modify. You can see that when there is no change in OPL, the second and third images become the same as the first image and the equation reduces back to its initial form.

From this equation, we can separate out the interference terms for each of the images into their own equations. We split k into the initial wavenumber, k_0, and any change in wavenumber, Δk, as this facilitates coherent summing into a single image. We then get two equations for the second and third image respectively:

$$I(k)_{middle} = e^{i(\varphi_{middle})}\sqrt{I_r(k)I_s(k)}\alpha e^{i2kz}e^{i\Delta k\Delta z(n-1)} + CC$$

$$with\ \varphi_{middle} = k_0\Delta z(n-1) + k_0\delta z$$

$$I(k)_{bottom} = e^{i(\varphi_{bottom})}\sqrt{I_r(k)I_s(k)}\alpha e^{i2kz}e^{i2\Delta k\Delta z(n-1)} + CC$$

$$with\ \varphi_{bottom} = 2k_0\Delta z(n-1) + 2k_0\delta z$$

We can use these derived equations to modify and coherently sum the images. First we depth decode the images by modifying the term that involves the change in OPL and then we modify the phase constant (which involves dz) in both images. The depth decoding factor should correspond to the OPL and, therefore, the value for the bottom image will be twice that of the middle image. Theoretically, we should be able to predict these values but, in order to maximize the resolution, we simply use an iterative method that finds the best values. The same method is used to find the ideal values for the phase constants.

This technology has been demonstrated to work in an OCT system to increase intensity over a larger DOF. However, our lab also utilizes methods for image resolution that involves phase. So beyond applying this technology to our system to improve the resolution over a larger DOF, we would also like to ensure that the phase is still useable and, hopefully, improved. We know the SNR corresponds directly to phase noise. We can use this relationship to analyze how phase data changes as a consequence of the annular phase plate.

Results and Analysis

Synthetic Aperture Initial Tests

We initially tested the system using plain glass slides and drilling a 0.5 mm hole in the center. We found that we were able to detect two separate images but that they were exceptionally close together. (Figure 5a)

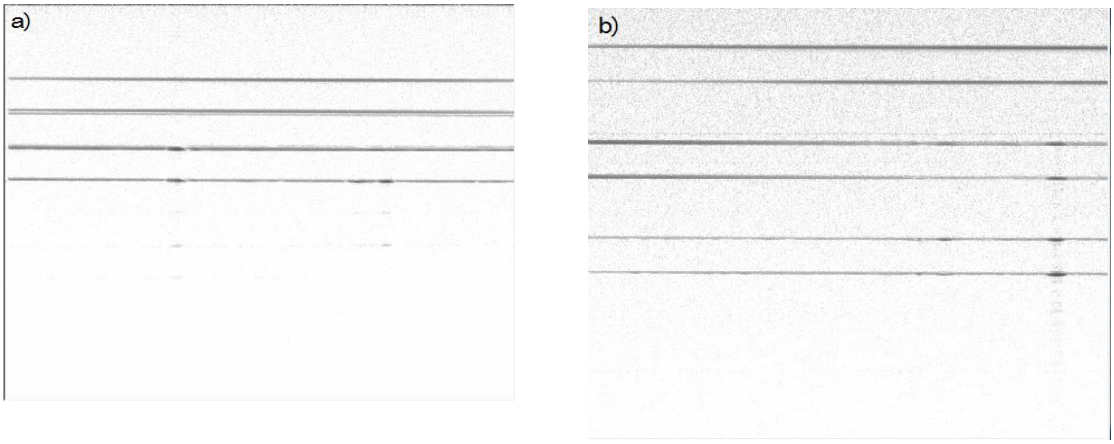

Figure 5: OCT images of glass slide obtained with synthetic aperture: a) 1mm glass; .5mm hole; 1300 system; $\Delta z(n-1)$ = .52mm; b) 2.3mm glass; .7mm hole; 1300 system; $\Delta z(n-1)$ = 1.19mm

We understood that this meant that the glass was too thin (creating a short change in path length) and so we ordered some thicker optical quality glass from Edmund Optics. The thicker glass produced images with a larger separation (Figure 5b). From this recording, we were able to obtain information about the intensity distribution of the images. (Figure 6).

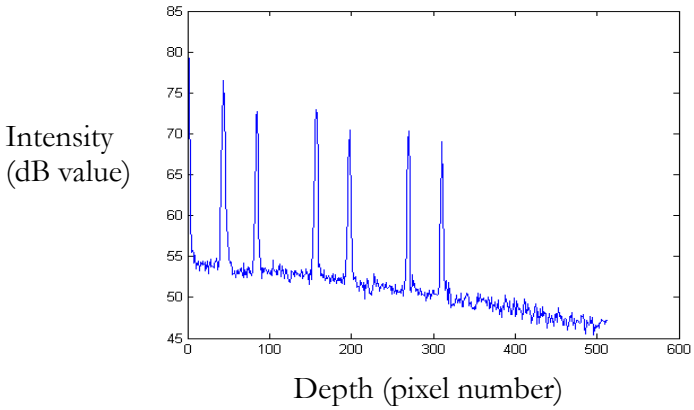

Figure 6: Intensity of all three images. From left to right, we have an increase in depth caused by the annular phase plate. 2.3mm glass; .7mm hole; 1300 system

As demonstrated earlier, we can use Equations 1 and 2 and the known parameters of the laser source to calculate the ideal hole size for image separation. With a more ideal hole size, we expect to see a more equal distribution of intensities across the three images. Following the procurement of this data, we gathered data more specifically on the relative intensity of only the top two images. The synthetic aperture technology is designed to collect different information from three different images and manipulate and combine said data to maximize the intensity.

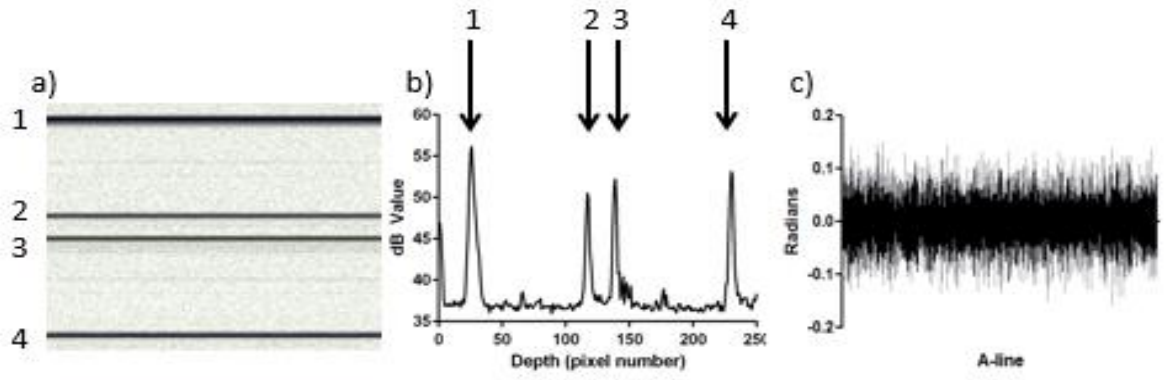

Figure 7: a) OCT image of glass slide with synthetic aperture; only two of the three images are shown. b) Plot of the intensity values of the two images as a function of depth. It can be seen from these images that the intensity across the images varies as a function of the change in path length. c) Overlap of the phase noise from the two images

As can be seen in Figure 7b, the intensity varies across the image as a function of the change in path length. We can use this variation in intensity to form a final image with a greater overall resolution. In this figure, for example, we would like to take information from point 1 of the first image and point 4 of the second image to form a new image with a higher SNR.

As mentioned earlier, we do not want to only maximize intensity, we would also like to see the effect this technology has on phase. In Figure c, we see that the phase noise between the two images is similar, which gives us a good indication that this is the case. To quantify this further, we use the known mathematical relationship between SNR and phase, which is given as the following:

$$\sigma_{\Phi} = \frac{1}{2SNR}$$

Where σ_{Φ} represents the standard deviation of the phase. We can use this information to compare the trends between the standard deviation of the phase and the SNR of the first two peaks (which represents the top and bottom of the first image respectively) and compare this with the trend between the standard deviation of the phase and the SNR of the first and fourth peaks (which represents the top of the first image and the bottom of the second image). If the same trend is observed then we have evidence that the phase is maintained across the image before manipulation.

From the data gathered (Figure 8) we see that the phase trend does remain constant across both images. This is promising in that we know that the phase trend is not altered as a consequence of the annular phase plate. The next step then is to check if the phase is improved following the synthetic aperture manipulations.

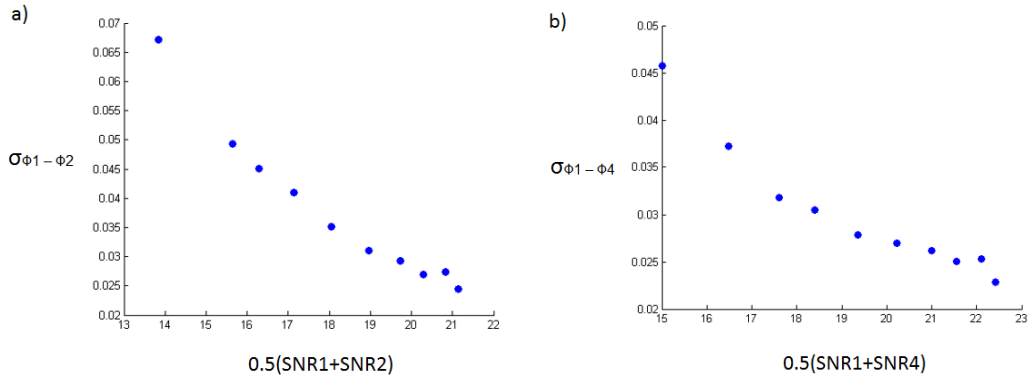

Figure 8: a) The comparison of the standard deviation of the phase vs the average SNR for peaks 1 and 2. b) The comparison of the standard deviation of the phase vs the average SNR for peaks 1 and 4.

Developing a New Apparatus

When the preliminary data was taken, the setup was rudimentary and lacked stability. Therefore, we developed a new apparatus that had a more stable arm for the annular phase plate, and also adopted other useful features not present in our earlier system, including a light based camera (Figure 9).

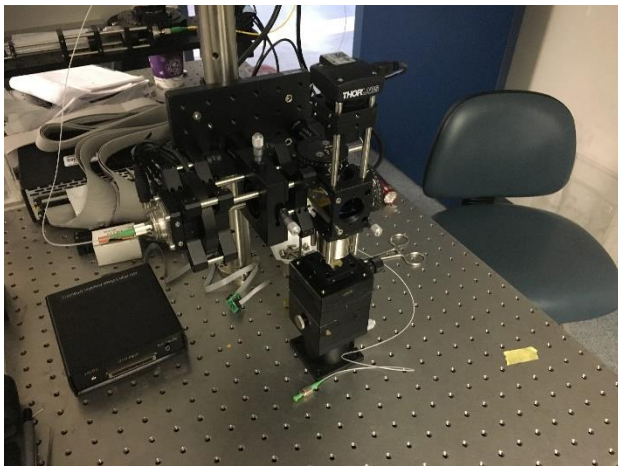

Figure 9: Picture of newly developed apparatus

Upon creating this new apparatus, we discovered issues with the scanning; consistent artifact was observed in the images taken (Figure 10). We proceeded to diagnose and address

this issue. After many tests were conducted, it was concluded that the artifact was being caused by issues with the input signal: the MEMS mirror works by using voltage changes to sweep the mirror across the desired angle. Originally, we were sending in a saw tooth wave to the MEMS mirror which was causing the return to baseline to occur too rapidly. This fast sweep was causing ringing of the MEMS mirror. To address this issue, I wrote code that would send in a modifiable wave which resembled a saw tooth but had a more relaxed return to baseline.

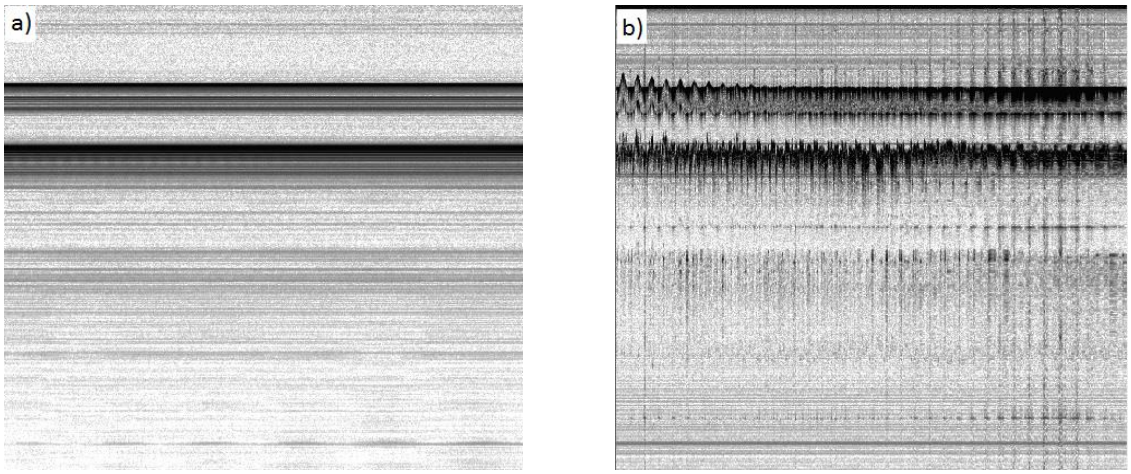

Figure 10: a) Image taken on new apparatus with no scanning. b) Image taken with scanning. Note jittery artifact.

The logic for the code is as follows: the wave is split into two functions: a linear function defines the initial sweep and a cosine function defines the return sweep. The slope of the linear function is defined by the user and determines how long the initial sweep is: the slope must always be greater than or equal to one, where a slope of one causes the sweep to cover all 2048 A-lines (which would lead to a sudden jump back to baseline and, therefore, be equivalent to a saw tooth). Any slope greater than one will cause the line to stop short of the full length of the sweep and an "if" statement then switches the function to a cosine function. The code is designed so that the linear function will always stop when the y-

coordinate of the linear function is equal to the input voltage (which should define the amplitude of the wave). The following cosine function is defined so that it will intersect with the linear function at the max point (input voltage) and be continuous. The cosine function then takes the wave back to baseline. The original code and obtained scanning is given in Figure 11.

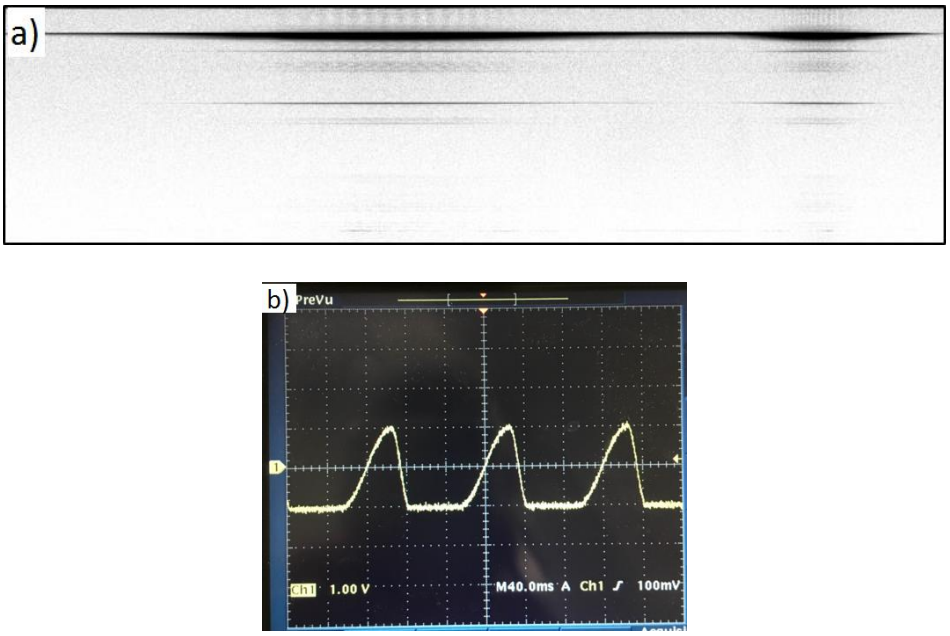

Figure 11: a) The scanning obtained with the new code; note that there is no remaining artifact. b) The waveform produced from the new code as recorded with an oscilloscope

The key to this code is rather than having a straight drop to baseline, as a saw tooth wave has, the cosine function should bring the MEMS mirror gently back to baseline. However, if the cosine is too steep, then we would have the same issue as previously demonstrated with the saw tooth wave. So we had to find the input value that yielded the longest range (largest sweep) and was still able to remove artifact. For an input voltage of one, this was found to be an input slope of 1.04. Further, we know that if we increase the

voltage, we will have a larger amplitude and, therefore, with the same slope, we will get a sharper return to baseline. This means that if we maintain the same slope value for higher input voltages, we will certainly obtain artifact. Therefore, the ideal value of 1.04 must increase as a function of voltage.

To find out exactly what kind of increase in the slope value needed, I took the derivative of the cosine function at the midpoint. This told us the acceptable rate of decline for the function that would yield no artifact and the maximum range. I then looked at what input slope would maintain, at least approximately, this value at higher voltages. A linear relationship was found in which an increase of one volt corresponded to an increase in the input slope of 0.05. The code was modified to include this.

Optimizing the Synthetic Aperture

As described previously, there are certain mathematical relations that govern the way light propagates through the synthetic aperture (see Background section). In order to obtain the best results from our synthetic aperture, we want to optimize the synthetic aperture so that we have an even distribution of the laser for all three images, which directly relates to the hole size, and we want to obtain a separation of images that allows for maximal size with no overlap, which directly relates to the thickness of the aperture. This optimization present two separate problems, both previously described.

For the first problem involving the diameter of the hole, we have obtained a theoretical value of 0.42 mm. In order to test this theoretical value, drill bits of 0.4 mm were ordered and a synthetic aperture was constructed using this drill bit.

For the second problem, glass was ordered of a few different thicknesses and the separation of the images was quantified. The total size of the imaging field was known to be

3 mm. With this knowledge, we could create ratios of images to the total field to find the physical size of what we were imaging. When imaging glass cover slips, as shown previously, we know that the optical path length should be greater than the physical size of the slip because glass has a higher index of refraction. Upon measurement however, we found that the optical size of the glass slide was not exactly what was expected. From this, it was gathered that the index of refraction could differ slightly in our system since the index of refraction is dependent on wavelength. To quantify this, I imaged a mirror and then imaged a mirror with a coverslip on top of it; the mirror movement in the image corresponded to the change in the optical path, which would then allow me to quantify the index of refraction of the glass in our system. The index of refraction, using this method, was found to be 1.42, a bit less than the literature value for glass. This new found value for the index of refraction reconciled the obtained data; the measured size of the obtained image for the glass cover slips matched the predicted value and the total image size matched the known size.

Though this information was reconciled, a consistent discrepancy between the measured separation of the images and the predicted value based on the thickness of the synthetic aperture was noted; the measured separation always fell short of the predicted value. In order to optimize our synthetic aperture, this has to be understood so that a synthetic aperture could be designed to yield an ideal image separation.

Recombination of separated images: Intensity Information

As was demonstrated previously,[1] implementing a synthetic aperture into an OCT system can allow for the manipulation and recombination of said images which results in a higher resolution for the image. The logic behind this method involves the known defining mathematical equations surrounding OCT. Based on these equations, when we cause a

separation within the image based upon an optical path difference, we obtain additional exponentials which contain both the optical path difference, $\angle z(n-1)$ for the first image and $2\angle z(n-1)$ for the second image, and the change in wave curvature, dz. We can then use these new variables to first manipulate the optical path difference and "depth decode" the two additional images. Finally we can manipulate the wave curvature dz and recombine the images to obtain a new image with an increased resolution.

The code that performs this task first performs the depth decoding. Theoretically, the values for this step should be equivalent to $\angle z(n-1)$ for the first image and $2\angle z(n-1)$ for the second image. However, theory often deviates from practice and the best way to find the values that will depth decode the image is algorithmically running through all possible values, which fall between 0 and 2π, and finding which values yield the best overlap. What we find is that the values found don't quite match up with the predicted values, though the value for the second image is twice the value for the first image, as expected (Figure 12).

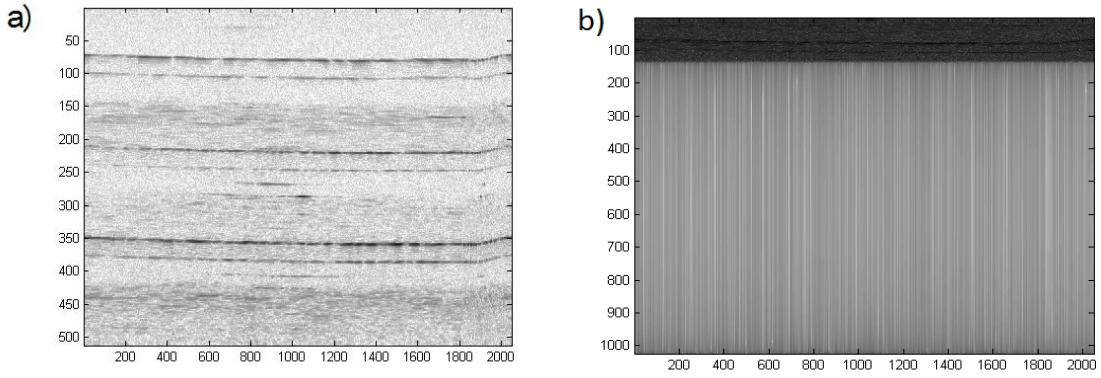

Figure 12: a) The three separated images before depth decoding. b) The three images recombined after depth decoding.

Once we have one recombined image through depth decoding, we remove the left over noise by limiting the range to the size of the image. Once in this form, we can modify the phase constant, which contains the wavefront curvature variable, dz, through a similar process. To find this value we plug in all possible values, which again fall between 0 and 2π, and find which value yields the highest value for the coherent sum, which yields the image with the best resolution (Figure 13).

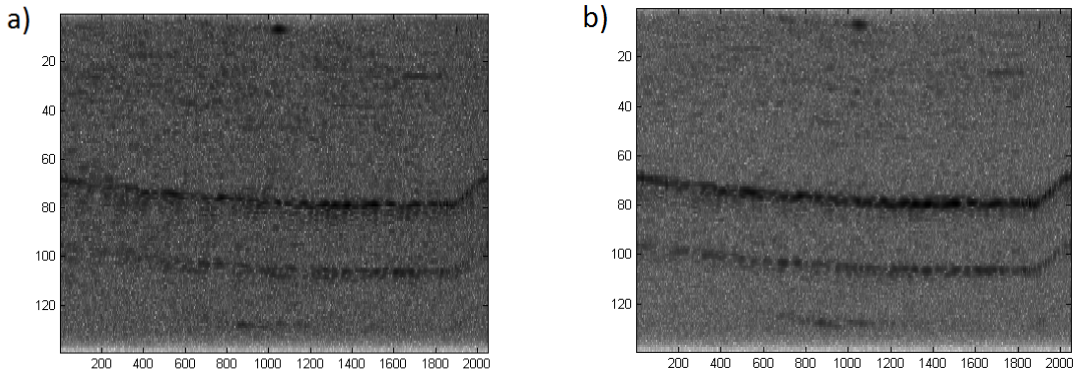

Figure 13: a) The recombined image before phase manipulation. b) The recombined image following phase manipulation.

Though the second image looks better than the first, a better quantification of the increase in SNR is by looking at the standard deviation of the phase. A smaller deviation, as demonstrated previously, correspond to a better SNR and, thus, a better resolution (Figure 14). From this data, it is clear that phase manipulation following the use of the synthetic aperture allows for an improvement upon the resolution of the image

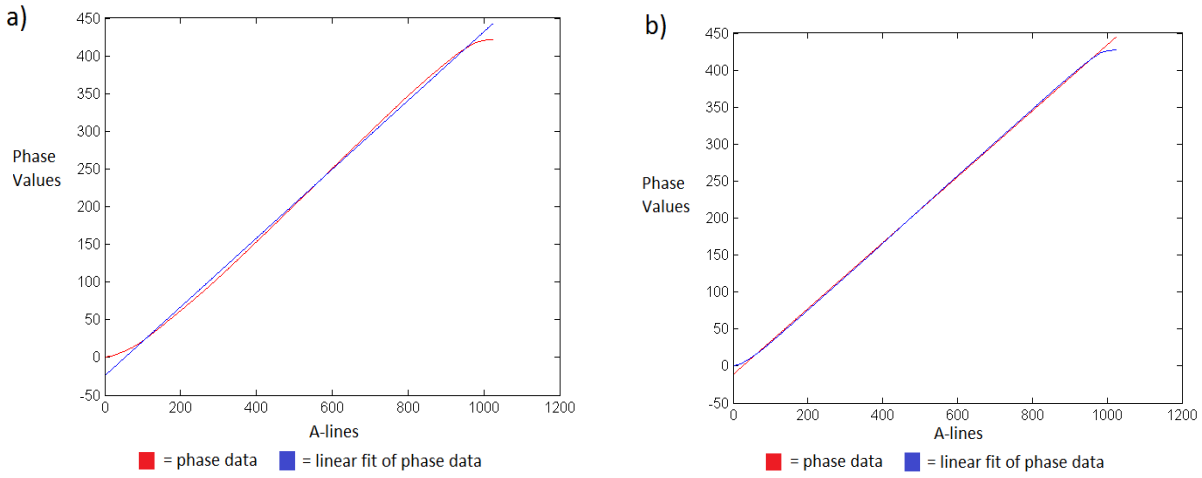

Figure 14: a) Phase data vs. linear fit for image before phase manipulation. b) Phase data vs. linear fit for image after phase manipulation.

Recombination of separated images: Phase Information

After demonstrating that we can indeed emulate the results from previous studies and increase the resolution of our images through phase manipulation, we wanted to observe what effect this has on the phase information, as phase is useful for our purposes. To understand this, we compared the phase information of the peaks between the image without the synthetic aperture in place to the phase information from the final processed image utilizing the synthetic aperture.

There is a known relationship between the SNR of an image and the standard deviation of the phase difference between two points, also known as the phase noise. This relationship is given as follows:

$$\sigma_{\varphi_1-\varphi_2} = \sqrt{\frac{1}{2SNR_1} + \frac{1}{2SNR_2}}$$

Where $\sigma_{\varphi_1-\varphi_2}$ is the standard deviation of the difference in phase between two depth locations and SNR_1 and SNR_2 are the SNR values at depth locations 1 and 2 respectively. We

can use recorded SNR values then to calculate the "ideal" values for the standard deviation of the phase. By comparing these theoretical values to those found from the data, we can know how closely our phase information aligns with the best possible values.

Upon first observations, it seemed that the recombined images had worse phase noise than the individual images, which is what is typically expected. Since we would like to minimize the phase noise as much as possible, code was designed that would focus on improving the phase noise of the image rather than the intensity. The code was successful in fulfilling this purpose and, interestingly, also yielded slightly better intensity information than the code that focused purely on intensity (Figure 15). Based on these findings then, we should utilize this new code for future experiments.

Conclusion

Improving the resolution of our system is very important for our purposes as we are trying to utilize OCT to image neurons, which are on the scale of microns. Furthermore, we would like to be able to use OCT to measure neural activity which is made possible by nanometer changes in the size of the neuron that occurs during activity and changes the optical properties of the tissue. Based on previous findings, the best way to increase our resolution was through the use of a synthetic aperture technology method which involved an annular phase plate and phase manipulation. In consideration of our purposes with phase, we also wanted to see what effect this technology had on the useable phase data.

As shown in this paper, we were able to not only emulate the previously demonstrated results and increase the resolution of our images, but we were also able to increase the useable phase values. Interestingly, when applying the algorithm to minimize phase noise and increase in the intensity was also observed. Whether or not this was a result

of an issue with the original intensity algorithms or if the phase code is just an altogether better method remains to be seen. Using this technology, moving forward, we hope to image and detect neurons and neural activity respectively.

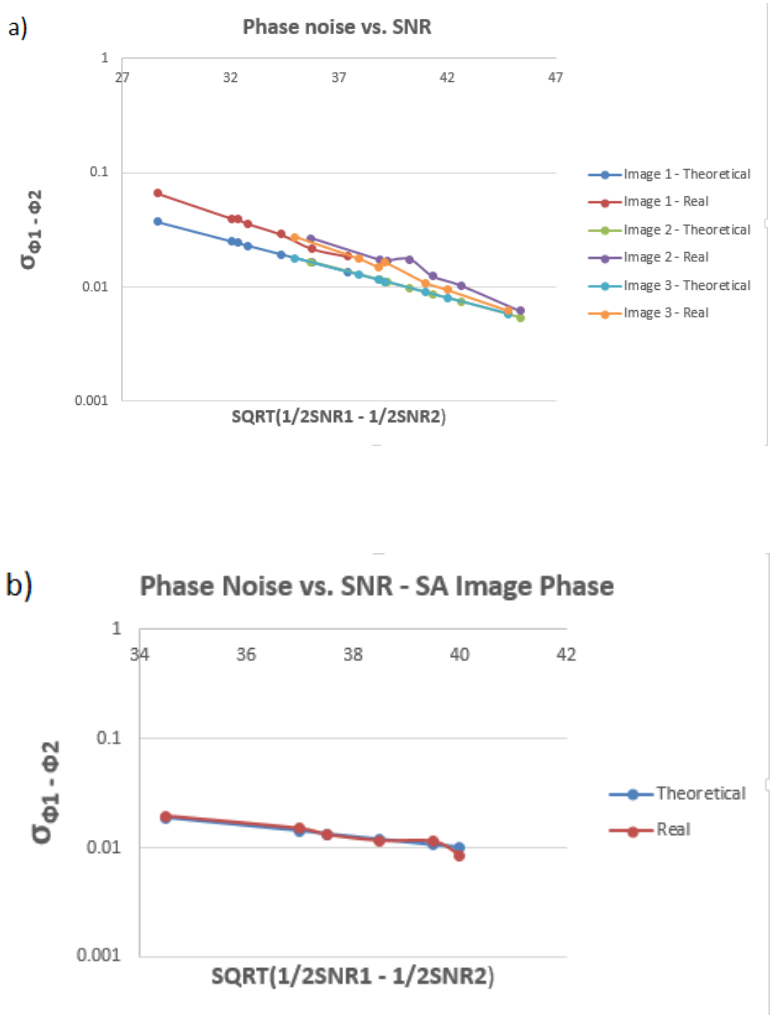

Figure 15: a) Comparison of theoretical phase values for individual images to recorded values. b) Comparison of theoretical phase values to recombined image using phase-focused manipulation algorithm

References

1. Mo, Jianhua, Mattijs de Groot, and Johannes F. de Boer. "Focus-extension by depth-encoded synthetic aperture in Optical Coherence Tomography."*Optics express* 21.8 (2013): 10048-10061.

2. Mo, Jianhua, Mattijs de Groot, and Johannes F. de Boer. "Depth-encoded synthetic aperture optical coherence tomography of biological tissues with extended focal depth." *Optics express* 23.4 (2015): 4935-4945.
3. Huang, David, et al. "Optical coherence tomography." *Science* 254.5035 (1991): 1178-1181.

4. Takarada, Shigeho, et al. "Advantage of next-generation frequency-domain optical coherence tomography compared with conventional time-domain system in the assessment of coronary lesion." *Catheterization and Cardiovascular Interventions* 75.2 (2010): 202-206.

5. Fercher, Adolph F., et al. "Measurement of intraocular distances by backscattering spectral interferometry." *Optics Communications* 117.1 (1995): 43-48.

6. Chinn, S. R., E. A. Swanson, and J. G. Fujimoto. "Optical coherence tomography using a frequency-tunable optical source." *Optics letters* 22.5 (1997): 340-342.

7. Siegman, A. E. (1986). *Lasers*. University Science Books. pp. 664–669. ISBN 0-935702-11-3.

8. Spring, Kenneth, and Michael Davidson. "Depth of Field and Depth of Focus." *www.microscopyu.com*. N.p., n.d. Web. 2016. <http://www.microscopyu.com/articles/formulas/formulasfielddepth.html>.

9. Rottenfusser, Rudi, Erin Wilson, and Michael Davidson. "Education in Microscopy and Digital Imaging." *http://zeiss-campus.magnet.fsu.edu/*. N.p., n.d. Web. 2016. <http://zeiss-campus.magnet.fsu.edu/articles/basics/resolution.html/>.

10. Zebker, Howard A., and Richard M. Goldstein. "Topographic mapping from interferometric synthetic aperture radar observations." *Journal of Geophysical Research: Solid Earth* 91.B5 (1986): 4993-4999.

11. Ralston, Tyler S., et al. "Interferometric synthetic aperture microscopy." *Nature Physics* 3.2 (2007): 129-134.

Chapter 2

Introduction

Phase measurements can be utilized to measure neural activity due to changes in the optical properties of the tissue during activity. It is understood that the detectable optical patterns happen as a result of volumetric changes. What causes these volumetric changes to occur, however, is not clear. Various hypotheses have been proposed[1, 2, 3] though no conclusion has been reached. From the literature, we gather that the volume change that occurs is typically on the order of $10^{-6} – 10^{-7}$ of the magnitude of the baseline volume (Table 1). Using this information, we can assess if specific models can explain the observed change in volume. In this chapter, I will analyze various hypotheses in this context and try to develop a fuller explanation of the phenomenon through mathematical computation and reference to the current literature.

Paper	Corresponding Distention (μm)	Corresponding Volumetric change (mm^3)	Original volume (mm^3)	Magnitude of volumetric change ((original – change)/ original)
Hill (1950)[4]	0.11	$7.6x10^{-8}$	0.57	10^{-7}
Cohen (1973)[5]	0.04	$2.8x10^{-8}$	0.57	10^{-7}
Tasaki and Byrne (1990)[6]*	0.31-0.83	$1.0\text{-}2.6x10^{-6}$	11.78	10^{-7}
Kim et al (2007)[7]	0.005 – 0.01	$2.0–3.0 \times 10^{-9}$	11.78	10^{-10}

Table 1: Volume change of nerves from literature. If values for nerve size were not given directly in paper, sizes were estimated based on experimental setup and literature. Volume values were converted to a common scale in which the volume change was compared to the overall volume of the cell. The volume change was assumed to take place over 1 micron of neuron (the area of activity), the length of the nerve was assumed to be 15mm unless otherwise specified, and the diameter was assume to be 1mm unless otherwise specified.
*This paper looked at volumetric changes by measuring the changes in the volume of water surrounding the cell, thereby removing any water component

Background

Water Flux Hypothesis

When volumetric changes were first observed, they were thought to be directly a consequence of water flux and, to this day, much of the literature on the subject suggests that neuronal swelling is solely a result of this flux.

One study attempted to correlate water influx with the optical activity observed and created various experimental set-ups to demonstrate this.[7] In one of these set-ups, the neuron was placed in a solution that was hypertonic to the cell. This means that, regardless of changes in the intracellular sodium or potassium concentrations, water should have a tendency to leave the cell. However, within this experimental set-up, swelling was still observed, though it was reduced in magnitude. The authors still concluded, however, that the swelling was a result of water influx.

Another group measured the swelling of a neuron through expansion of the fluid medium surrounding the cell.[6] By measuring the expansion of the fluid, the authors noted that any changes in the size of the neuron could not be attributed to water influx as this would cause the extracellular volume to proportionally decrease, causing overall no measured volume increase, implying that the expansion was caused by more than simply water influx.

Most experimentation has demonstrated that the swelling of the neuron is typically on the order of about 10^{-6} - 10^{-7} of the original size of the cell (Table 1). In order to best understand if water can account fully for this change, we can mathematically model the flux and estimate the magnitude of change that would result from it.

Thermal Expansion of Axoplasm

There is a known and recorded temperature change associated with action potentials. It is thought that this change in temperature could be responsible for a thermal expansion of water which could then be responsible for the volumetric change. One paper, however, specifically states that this hypothesis is highly unlikely since the known temperature change should correspond to a negligible change in volume.[2] We can analyze this hypothesis by using established mathematics for water expansion and see if the estimated expansion could explain the measured change in neurons.

Kinetic model

When a neuron is activated via transmitter, channels will open causing a depolarization of the cell. If this depolarization exceeds threshold, voltage-gated Na^+ channels open. Because of the resting negative potential of the cell, Na^+ ions will rush inward. The Na^+ ions then propagate down the axon causing further opening of voltage-gated Na^+ channels (Figure 1a). This activity has been shown to correlate directly with a change in the volume of the axon as well as a change in temperature. When the voltage-gated channels are open, the potential energy in the resting state is converted to kinetic energy associated with these ions. I hypothesize that this kinetic energy could cause increased pressure within the cell which could cause increased collisions with the walls of the axon. These collisions then can impart energy onto the walls causing an expansion, reminiscent of the classical relationship PV=nRT (Figure 1b). I hope to prove or disprove this hypothesis through mathematical analysis.

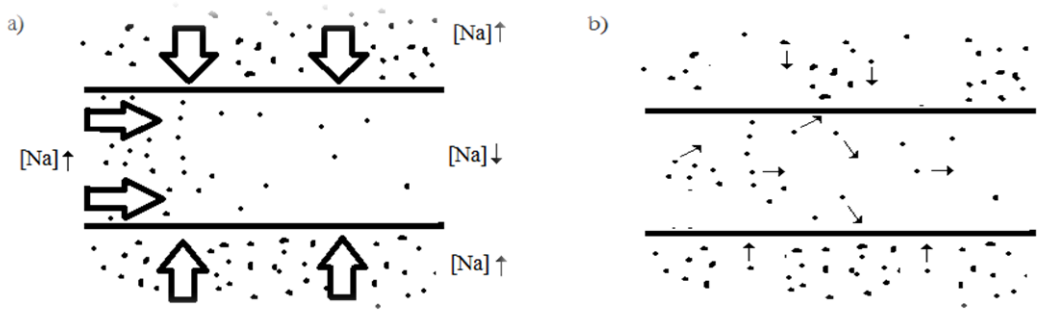

Figure 1: a) Model axon drawing that shows the general flow of Na+ ions down their concentration and voltage gradient from the left and the outside of the axon to the right and inside the axon respectively. b) Demonstrates the general movement of ions down their concentration gradient with some random movement caused by collision and interaction.

Phase Change Hypothesis

Ichiji Tasaki made valuable contributions to the study of neuronal swelling across his more than fifty years of research on the subject. In this time, he developed an idea, based on the empirical evidence he had gathered, as to how this swelling might be occurring: Tasaki observed that the levels of Ca^{++} in a solution and, more specifically, the ratio of Ca^{++} to Na^{+} ion, could affect the cell's swelling.[7, 8] Tasaki hypothesized that Ca^{++}, under normal circumstances, would interact with the anionic groups of the phospholipid bilayer, allowing for greater stability of the bilayer. When there was an influx of Na^{+} during activity, the increased concentration of Na^{+} near the surface would cause displacement of Ca^{++} ion and replacement by Na^{+} ion. Because Na^{+} has half the charge Ca^{++} has, the interactions it possesses with the anionic groups would be weaker, causing decreased interaction which allowed for increased movement normal to the membrane leading to membrane expansion. In his later work, Tasaki showed further that, while varying the Ca^{++} to Na^{+} concentration, there was a very sudden jump in thickness, indicating a more sudden phase change. Based on other work, it was hypothesized that at this point, the phospholipid bilayer had "loosened

up" to a threshold that allowed water to fill in between the layers, causing a sudden jump in expansion.[9]

This phase change can be related to another recently proposed hypothesis in the field of neuroscience: the soliton hypothesis.[10] The soliton hypothesis purports that neuronal signals are propagated by a phase change in the membrane, from a "fluid" to a "gel" phase. From a thermodynamic perspective, this phase change can act as a self-propagating wave, leading to the term "soliton." This hypothesis is made in contrast to the Hodgkin-Huxley hypothesis which purports that the signal is transduced by the influx of ions through voltage-gated channels. This hypothesis provides explanations for certain phenomenon that the reporters believe the Hodgkin-Huxley model doesn't adequately explain, namely volume changes, temperature changes, and anesthetic effects. It is the opinion of this author that a phase change may occur during activity, but this phase change is a consequence of signaling rather than a mechanism of signaling.

Flexoelectricity model

Another proposed hypothesis involves a change in the membrane caused by the voltage change during activity. Flexoelectricity is an observed physical phenomenon in which a strain on a solid causes a polarization. The converse flexoelectric effect then is when a voltage change causes bending of a solid. It is proposed that during the action potential the change in voltage results in a converse flexoelectric effect which can cause folding of the membrane.[11] This implies that the volume change observed is a consequence of curving of the membrane during activity. The flexoelectric effect in the context of cells was put forth as an explanation to physiological bending of cochlear hair cells[12] and later proposed as a possible explanation for observed optical activity.[3]

Analysis

Water Flux Hypothesis

In a paper on the subject, a group used modified versions of the Hodgkin-Huxley equations to demonstrate that the volumetric changes of the cell correlated well with the measured optical activity.[1] Though the authors did not make the magnitude of the volumetric changes the focus of their paper, this information can be obtained from the given equations.

By plugging in the derived differential equations and using an ODE45 solver, we obtain the solutions below which reflects the results discussed in the original paper (Figure 2). There is an increase in the overall volume of the cell during the rising and most of the falling phase. During the hyperpolarization, however, we see a slight shrinkage of the cell. At the peak of expansion, which occurs around -55 mV during the falling phase, the change in volume obtained is 5.59×10^{-21} m^3. We have an input volume of 5.24×10^{-16} m^3 which means that the magnitude of the change is on the order of 10^{-5}.

However, a volume of 5.24×10^{-16} m^3 is completely unrealistic for a neuron with a diameter of 10μm, as was given in the paper. This would essentially result in a neuron that is 1μm long. This would make sense if we were looking at just the area of the activity, which might be appropriate for their mathematical model, but this would then not reflect the overall volume change but rather the volume change at the area of activity. A more realistic volume for a neuron of this size is on the order of 1×10^{-12} m^3. However, with a larger and more realistic volume for the cell, the volume actually decreases as a function of time which is caused by the fact that the flux of ions is based on the overall concentration and a higher volume would change the overall concentration, which indicates the model is dependent on

focusing on the smaller area where activity is occurring. Though the model does appropriately demonstrate an action potential and the corresponding volume changes, if we consider the total measured volume changes in reference to, what should theoretically be, the entire cell, the magnitude is much smaller, around 10^{-9}. Since the literature shows a change more on the order of $10^{-6} – 10^{-7}$, even when water effects are excluded,[6] it seems water plays only a minor, if not negligible role, in the overall change.

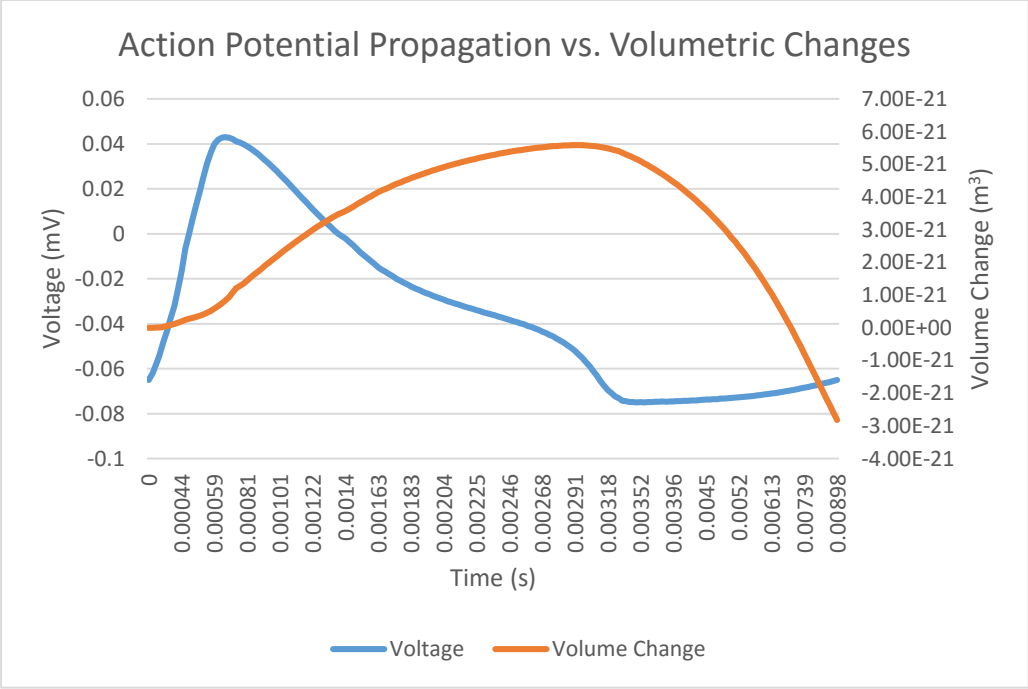

Figure 2: Action potential modeled in MATLAB using modified Hodgkin-Huxley equations. Voltage changes are plotted against volumetric changes as a function of time for an initial volume of 5.24 x 10^{-16} m^3

Thermal Expansion Hypothesis

We can mathematically evaluate this hypothesis since the thermal expansion of water is well understood. The equation for thermal expansion is given by

$$dV = V0\,\beta\,(\Delta t)$$

Where V is the volume, β is the volumetric expansion coefficient, and Δt represents the change in temperature. The maximal change in temperature according to the literature is around 2.3 x 10^{-5} °C.[2] The coefficient for water is given as 2.07 x 10^{-4} $^{o}C^{-1}$ at room temperature. Regardless of the initial volume, these two coefficients will cause the same magnitude of change which comes out to 10^{-9}. Because the overall volumetric change is on the order of 10^{-6} – 10^{-7}, the volumetric change associated with temperature is small if not negligible.

Kinetic Hypothesis

In order to test if Na^{+} influx can cause distention of the axon, we first test to see if the force generated by these ions can cause distention neglecting all other forces. In order to understand this problem, we must look at the material properties of the axon membrane. A model has been developed in previous work for the force required to distend a membrane.[13] The equation takes the following form:

$$F = k\left(\frac{L_x}{2}\right)\theta^3 + 2T_0\theta \qquad (1)$$

Where k is the elasticity, L_x is the length of axon being distended, θ is the angle of distention, and T_0 is the initial tension on the membrane. These values correspond to a geometry as shown in Figure 3. The values of k and T_0 were found to be 0.1 - 0.7 mN m^{-1} and 0-2 nN respectively. L_x would be the length specific to our problem. Since we are

looking at the distention of the membrane caused by a Na^+ ion, it makes sense for us to use the diameter of a Na^+ ion which is about 0.18 nm. θ is the angle that corresponds to the amount the axon is distended. The literature tells us that, during activity, the neuron is distended between 1.0×10^{-6} and 2.6×10^{-6} mm^3.[6] This is a 3D value however and our model requires a 1D value. To convert from volume to area we first divide by the total length of the axon which in our model, which approximates the literature, is about 15 mm. To go from area to length we need to divide this area by the total circumference of our axon which in our model is about 0.314 mm (the radius is 50 μm). Dividing our original values by these two values gives us a total distention of 0.21 - 0.55 μm, which corresponds well with finding of Hill.[4] Modeling the distention of the membrane as a right triangle with the height equal to the total distention and the base equal to half of our L_x value we find that θ is equal to 89.75^0 - 89.90^0 (or 1.57 in radians). Now we have all the values we need for our equation. If we plug them in we find that the force needed to generate the distention needed in our problem is 3.48×10^{-14} N – 6.00×10^{-9} N. This is a very large range but is based on the parameters given for our problem. We should notice though that the T_0 term has a large effect on the upper values of our force and, if this term is neglected, the range is 3.48×10^{-14} N – 2.43×10^{-13} N which is appreciably smaller range.

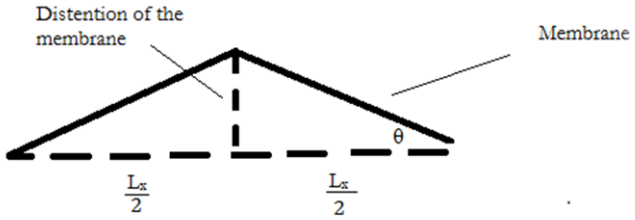

Figure 3: The geometrical model of membrane distention that explains equation (1)

Now that we have found the force needed to distend our membrane, we need to see if a Na^+ ion traveling down its gradient will have enough force to cause this distention. There are two forces acting on a Na^+ ion when it is moving down its concentration gradient: the electrical gradient and the concentration gradient. Both of these forces are described by the Nernst-Planck equation with the time derivatives set to zero as follows:

$$J = -\left[D\nabla c + \frac{Dze}{k_b T} c(\nabla \Phi)\right] \qquad (2)$$

Where J is the flux, D is the diffusivity, c is the concentration, z is the valence of the ion, e is the elementary charge, k_B is the Boltzmann constant, T is the temperature, and $\nabla\Phi$ is the potential difference. Since we are modeling movement in one dimension, we can replace the gradient with a change in one dimension; we will use x here. The diffusion coefficient for Na^+ in axoplasm is 0.65×10^{-9} - 1.3×10^{-9} m^2s^{-1}.[14] Voltage-gated Na^+ channels open around -50 mV and so we define the potential difference as such for our model. We will assume a standard temperature of 25^0C. Plugging our constants into our equation we get a simplified version:

$$J = 1.27\ x\ 10^{-9}c + 6.5\ x\ 10^{-10}\frac{\partial c}{\partial x} \qquad (3)$$

Now we must define the concentration in our problem. A typical neuron has a $[Na^+]_I$ of 12 mM and a $[Na^+]_o$ of 120 mM. We are looking at flux across this membrane and so we choose a point on the inside. At this point our concentration will be 12 mM. The derivative of the concentration with respect to our position is a consequence of the difference between the inner and outer concentrations and the distance between them, namely the membrane thickness. We will estimate the membrane thickness to be 4 nm. From these numbers we get that J = 0.01755 mol m^{-2} $s^{-}1$. This tells us how many moles of Na^+ are flowing in through a channel as a function of area and time. We know that the molar mass of sodium is 22.99 g mol^{-1}. Using these values we obtain a mass flux of 0.403 g m^{-2} s^{-1}. With this mass flux, we can then find the velocity of the particles using the vector definition:

$$J = \rho v \quad (4)$$

Where J is the flux vector, v is the velocity vector (pointing in the same direction as the flux), and ϱ is the density. The density of Na^+ is 0.968 g cm^{-3} (or 968 g m^{-3}). With this value we find the velocity on the particles to be 4.17 x 10^{-4} m s^{-1}.

The kinetic energy on each of these atoms can be expressed by the relation:

$$KE = \frac{1}{2}mv^2 \quad (5)$$

Where KE is kinetic energy, m is mass, and v is velocity. With this relation we find the kinetic energy on any individual Na^+ ion to be 1.20 x 10^{-28} J. Energy can do work where work is force times distance. We know from our previous calculations that we need 3.48 x 10^{-14} N – 6.00 x 10^{-9} N to move the membrane a distance of 0.21 - 0.55 μm. If we take our

KE divided by this distance we obtain a force of $\underline{2.18 \times 10^{-22} - 5.71 \times 10^{-22}}$ which is not within our range.

This preliminary problem shows us that, without consideration of any drag forces, our sodium ions are unlikely to be able to provide enough force to distend the membrane.

However, to further quantify what magnitude this phenomenon plays in the swelling, if any, the next thing to look at are the drag forces acting on the Na^+ ions. The drag force is defined by the equation:

$$F_D = \frac{1}{2}\rho v^2 C_D A \quad (6)$$

Where ρ is the density of the fluid, v is the velocity of the particles relevant to the fluid, C_D is the drag coefficient, and A is the cross-sectional area of the particle. The fluid our particle is moving through is axoplasm. From the literature, we know axoplasm has a density of 0.31 g cm^{-3}.[15] During activity, the axoplasm should not be flowing but rather the ions should be flowing relative to the axoplasm which means our velocity value will be directly a consequence of the velocity of the particle. The drag coefficient can be estimated from the literature.[16] We model our particle as a smooth sphere but we must find the Reynold's number to know precisely what to model the coefficient as. The Reynold's number can be expressed as follows:

$$Re = \frac{vD}{\nu} \quad (7)$$

Where v is the velocity, D is the characteristic diameter, and ν is the kinematic viscosity. From the literature we find that the dynamic viscosity is 1 mPa s^{-1}.[17] The kinematic viscosity can be obtained by dividing the dynamic viscosity by the density of the fluid (stated earlier to be 0.31 g cm^{-3}). This gives us a kinematic viscosity of 4.03×10^{-7} m^2 s^{-1}. The

characteristic diameter is relevant to the diameter of whatever the fluid is flowing through. In our model, we will make this equal to the diameter of the Na^+ channel which we know to be 0.4 nm. Using the velocity we found previously, we find our Reynold's number to be 4.13 x 10^{-7}. We can then plug this into our equation for the drag coefficient which is:

$$C_D = 4.5 + \frac{24}{Re} \quad (8)$$

Using this we find a value for our drag coefficient of 5.81 x 10^7. Finally, we need the cross-sectional area of our particle which we can find using the atomic radius. We know the atomic radius of Na to be 0.19 nm. We can use this to solve for the cross-sectional area using the formula for the area of a circle. We find the cross-sectional area to be 1.13 x 10^{-19} m^2. Now we can calculate the drag force to be 1.77 x 10^{-13} N at the given velocity.

In order to find out the force that our Na^+ ion will produce after passing across the axon we first divide our force by the mass of the Na^+ ion. This tells us the negative acceleration acting on the particle. We find a negative acceleration of 1.27 x 10^8 m s^{-2}. So we can now write a velocity equation for our particle as follows:

$$v(t) = 4.16 \text{ x } 10^{-4} - (1.27 \text{ x } 10^8)t \quad (9)$$

We also know that the location of our particle in space can be described by the function:

$$x(t) = (4.16 \text{ x } 10^{-4})t - (.64 \text{ x } 10^8)t^2 \quad (10)$$

We find that this function has a maximum of 6.86 x 10^{-16} m at time 0.00042 s which is a much smaller distance than the diameter of our axon. However, we know that the drag force is directly proportional to the velocity. Thus as the velocity goes down, our drag force should also go down. This makes our model a bit more complicated and we can use some code to calculate this. I wrote a C++ program to calculate this value.

From our code, we see that the velocity and negative drag force balance out around 1.11×10^{-13} m. This is larger than our previously calculated value but still not nearly enough to traverse the axon.

If the ions coming into the cell are not able to traverse the axon, let alone distend the membrane, then what else could be causing this distension? We know, besides the sodium ions flowing into the cell, we have sodium ions flowing parallel to the propagation. These ions, after being accelerated by the voltage force, may have enough velocity to distend the membrane. Our path of interest begins inside the cell (after the sodium ions have entered through the dendrite and are moving towards the axon hillock) and, since the concentration change in the cell is negligible, we can ignore the concentration term. However, we do not want to just look at the flux at a point here but rather we want to look at the acceleration of the particles as they are continuously pulled towards a negative potential. To find the velocity on these flowing particles, we can look again at the electric field generated by the voltage. This electric field multiplied by the conjugate charge will give us an electrical force. The dendrite is about 800 microns from the axon hillock. We must also keep in mind that as the ions enter the cell they are themselves changing the voltage near them. For now we will focus on the first bit of Na^+ entering the cell which would have a negligible effect on the voltage. We know that -50 mV is around the voltage required to induce the opening of the voltage-gated ion channels so we will consider this to be the voltage surrounding our first bit of Na^+ ions. This ion will want to move towards the axon hillock with the more negative charge. This electric field can be described in terms of the voltage difference (15 mV) and the distance (0.8 mm) as 18.75 V/m. This electric field can then be multiplied by the charge on the ion to yield the force. We find this force to be 3.00×10^{-18} N. If we divide this force

by the mass of the ion we will find the acceleration imparted on it over this distance. We find the acceleration to be 2167.00 m s^{-2}. As the distance between the ion and the voltage decreases the force and consequently the acceleration will increase. To obtain an accurate expression we therefore have to use code again. Unfortunately the code for this model was cyclical and had some behavior that was hard to control; since the acceleration was dependent on the net force, the velocity was dependent on the acceleration, and the net force was dependent on the velocity, there was a point in the sequence in which the acceleration would become negative which would cause the net force to jump down which would cause the acceleration to jump down which would cause the net force to jump up which would cause the acceleration to jump up etc. in a sort of positive feedback mechanism that made the solution useless. Even though switches were implemented to make the code iterate until a solution was obtained, it is questionable whether or not this code resembled any physical reality since it involved changing the fundamental relations. The code tells us that the velocity at the end of the path is equal to 7.857 x 10^{-4} m s^{-1}. If we convert this value to kinetic energy and then to force we find that we have a force of 5.62 x 10^{-23} N across a distance of 0.21 μm, which is again not within our range.

We must consider further that this kinetic energy will not all be directly imparted onto the membrane. In fact, it will majorly be focused in the direction of the action potential with a tendency towards the center of the axon since the space near the membrane will be more immediately depolarized. We can consider the force imparted on K+ as it leaves the cell since these ions will be directed towards the membrane. However, it is unlikely that the K+ will have acquired any kinetic energy before exiting the cell through the channel. At a maximum value, the kinetic energy of the ions seems to play a negligible role in the overall

process and, based on the physical manifestation of the action potential, it is unlikely that this force will be directed at the membrane in a significant enough manner to play a relevant role in the distention.

Phase Change Hypothesis

The claim of a phase change induced by ionic flux during activity is well supported by the studies of Tasaki and others.[8,9] However, this theory does not lend itself very easily to mathematical quantification as far as what magnitude of effect such a transformation could have on the membrane. The best way to try to quantify such a problem would be to look at the difference between a Na^{+} and Ca^{++} ion in terms of the strength of the attraction to the phospholipids. Using this information we should be able to derive a difference in the bond length which can then be integrated across the membrane surface to find the total possible distention. However, the only way to model the differential pull of the ions is from the Lennard-Jones Potential or a similar expression. These expressions are able to give an energetic relationship with given distances but, since we are attempting to find the distance, it is not possible to use these relationships for our purposes. We would need to reference optical data on the subject. However, the literature on the subject is arcane and lacking. We know that ultimately the distance of the phospholipids is a consequence of the ionic interactions can be described in terms of Coulomb's Law. Therefore, Ca^{++}, which we assume to be the principle component bonding to the phosphate heads at baseline, will have twice the force of Na^{+}, all other things constant. So, if we look at the literature for the normal distance between phospholipids, if all other forces remain the same, we can estimate the change in packing to be twice the distance it is at baseline. Realistically, this is probably an overestimate of the difference that such a change would make, but it will help us understand

the possibility. From the literature, we find the baseline distance to be about 0.9 nm which means with a Na^+ ion associated, we would have a separation of 1.8 nm in our model. We assume in our previous calculations that the area of activity is around 1 μm in length. Since phospholipids are around 1 nm thick, we can imagine this activity could affect millions of phospholipids. A change in the phospholipid spacing of this magnitude could have a significant effect on the size of the membrane.

Unfortunately, there were many assumptions made for this modeling, primarily in the realm of the distance between phospholipids, and it is hard to say what bearing it has on reality but, due to the lack of literature on the subject, it is hard to be more precise.

We can, however, reference physiological data about the expansion effect of a phase change as observed in lipid membranes. According to the literature,[10] a phase change from the "fluid" to "gel" phase would result in approximately a 16% expansion of the membrane. In our model, the membrane is estimated to be 8 nm and so this corresponds to a change of around 1.3 nm. This, however, applies to all individual neurons within a nerve and, since there exists hundreds of neurons within a nerve, this magnitude of change is consistent with the literature.

One idea further proposed by Tasaki and colleagues was that the phase change allowed for increased spacing within the membrane which would allow for water to diffuse into the membrane, causing expansion. However, this idea would be in contrast to the data that showed the volume changes maintained a similar magnitude without the contribution of water.[6]

The authors who put forth the soliton hypothesis were unclear about mechanistic possibilities, and even the ionic hypothesis put forth by Tasaki was a bit vague. It is the

opinion of this author that the anionic residues that Ca++ associates with is most likely the phosphate heads of the lipids since these are in large quantity in the membrane and past experimentation supports the idea that Ca++ associates with these groups.

Though there is evidence demonstrating the possibility of this mechanism, the current physiological data suggests that the induced changes would not be sufficient to explain the observed changes in the membrane. Further evidence is needed to evaluate this hypothesis.

Flexoelectricity Hypothesis

Based on a previous model proposed for the flexoelectricity of membranes,[12] the change in voltage is related directly to the change in the longitudinal curvature by the following equation:

$$\Delta c = \frac{f \Delta V}{k_{eff} h}$$

Where Δc is the change in curvature in the longitudinal direction, f is a constant given as 10^{-18} – 10^{-20} C, k_{eff} is a constant given as 2 x 10^{-19} J, and h is the thickness of the membrane which we will assume to be 4 nm. Solving this equation we find that the change in curvature for a membrane depolarized by a 100 mV will have a resulting change of 625,000 – 125,000,000 m^{-1}, which corresponds to a radius of curvature 8 - 1600 nm. This is an incredibly large range, which comes mainly as a consequence of the large range for the constant *f*. From the literature, we know that the total length change of the axon is found to be in the range of 20-80 nm which should correspond directly to the arc length of the curve, assuming there is only one fold.[18] If we utilize the full range of values for the possible radius of curvatures, we find that the lower range of values for our radius of curvature does not

work, as the size of the arc then is greater than the possible circumference. Since we assume that this distention could, at most, compensate for half of the circle, we find that the minimum radius needed is in the range of 6.36 – 25.46 nm, dependent on the arc length of the distention. Using the radius of curvature in conjunction with the arc length, we can find the length of distention to be in the range of 0.03 - 25.46 nm. This is a very large range, spanning three orders of magnitude. Because again this value would correspond to individual neurons, it is possible that the magnitude of the change is within our range. We have to consider though that the magnitude of the change could be reduced with increased folds.

Beyond the math we have already looked at, we have to consider if this theory makes sense in consideration of the empirical evidence. Because voltage changes are inherent to any action potential and the flexoelectric effect is completely a consequence of voltage changes, it is impossible to remove the cause of this effect and still observe activity. However, we can consider at least one known change that must happen if the converse flexoelectric effect was to occur: **i**f the flexoelectric theory holds true, we should see a shortening of the axon during expansion since the curve in the membrane would pull both sides towards itself. Tasaki and colleagues did indeed observe a change in length that accompanied the volumetric changes,[2] lending further support to this hypothesis.

Conclusion

Although water flux has often been cited as the cause of the volumetric expansion of neurons during activity, the mathematical model for this phenomenon derives a theoretical value that is a few magnitudes smaller than what the literature suggests the volumetric expansion to be. Furthermore, a change in volume is still observed when water flux changes are removed either by measuring the changes as a function of water or eliminating the

driving force on water during activity. This implies that water may play a role in the change, but it is not the only contributor and likely not the major contributor.

The thermal expansion of water may play a small role, but is most likely negligible to the overall change. Kinetic effects induced by ion flux, after modeling, appear to be negligible compared to the overall change in volume as well.

The two most novel hypotheses to explain the overall change in volume observed, phase change and flexoelectric hypotheses, seem to be, based on our analysis, a reasonable explanation for the phenomenon, though understanding these phenomena was difficult based on the available information. Both the phase change and the flexoelectric hypothesis could reasonably explain the phenomenon based on this analysis so we must consider then, which of the two hypotheses to be the most likely. Is it possible that both factors are at play? Both phenomena would affect the membranous properties which could cause issues with for the other phenomenon. For example, the previous flexoelectric measurements may have been measured in the "fluid" like phase and a conversion to the "gel" like phase might cause less flexing. Conversely, the flexoelectric effect could change the spacing of phospholipids and affect the ability for a phase change to occur. It is, however, possible that both of these processes work in conjunction to yield the total change or that other changes in the membrane, such as changes in elasticity, also play a role.

It seems then that the two most novel hypotheses in regards to swelling may be the most accurate but further investigation of both phenomena are needed to understand their applicability to the action potential. The promising nature of these ideas in the context of the current literature on the subject suggests that the change in the volume of the cell is very likely attributed to changes in the membranous properties and, therefore, future studies

should focus on what kind of changes may occur and piecing apart which effects, whether it be the ones discussed here or elsewhere, may play a role in the membrane changes observed.

References

1. Lee, Jonghwan, and Sung June Kim. "Spectrum measurement of fast optical signal of neural activity in brain tissue and its theoretical origin." *Neuroimage*51.2 (2010): 713-722.

2. Tasaki, Ichiji, Kiyoshi Kusano, and Paul M Byrne. "Rapid mechanical and thermal changes in the garfish olfactory nerve associated with a propagated impulse." *Biophysical journal* 55.6 (1989): 1033.

3. Akkin, Taner, David Landowne, and Aarthi Sivaprakasam. "Optical coherence tomography phase measurement of transient changes in squid giant axons during activity." *Journal of Membrane Biology* 231.1 (2009): 35-46.

4. Hill, D.K. (1950) The volume change resulting from stimulation of a giant nerve fibre. *Journal Of Physiology* **111**, 304-327.

5. Cohen, L. B. "Changes in neuron structure during action potential propagation and synaptic transmission." *Physiol. Rev* 53.2 (1973): 373-418.

6. Tasaki, I., and P. M. Byrne. "Volume expansion of nonmyelinated nerve fibers during impulse conduction." *Biophysical journal* 57.3 (1990): 633-635.

7. Kim, G. H., et al. "A mechanical spike accompanies the action potential in mammalian nerve terminals." *Biophysical journal* 92.9 (2007): 3122-3129.

8. Tasaki, I., and P. M. Byrne. "Discontinuous volume transitions induced by calcium–sodium ion exchange in anionic gels and their neurobiological implications." *Biopolymers* 34.2 (1994): 209-215.

9. Tasaki, Ichiji. "Rapid structural changes in nerve fibers and cells associated with their excitation processes." *The Japanese journal of physiology* 49.2 (1999): 125-138.

10. Heimburg, Thomas, and Andrew D. Jackson. "On soliton propagation in biomembranes and nerves." *Proceedings of the National Academy of Sciences of the United States of America* 102.28 (2005): 9790-9795.

11. Todorov, A. T., A. G. Petrov, and J. H. Fendler. "First observation of the converse flexoelectric effect in bilayer lipid membranes." *The Journal of Physical Chemistry* 98.12 (1994): 3076-3079.

12. Raphael, Robert M., Aleksander S. Popel, and William E. Brownell. "A membrane bending model of outer hair cell electromotility." *Biophysical journal* 78.6 (2000): 2844-2862.

13. Bernal, Roberto, Pramod A. Pullarkat, and Francisco Melo. "Mechanical properties of axons." *Physical review letters* 99.1 (2007): 018301.

14. Arhem, Peter (1976) Diffusion of sodium in axoplasm of myelinated nerve fibre. *Acta Physiologica Scandinavia*. **97**, 415-425.

15. Hartmann, Henrik and Casapis, Michael (1967). Cytoplasmic and axoplasmic density variations in relation to hyperactivity. *Acta Neuropathologica*. **7**, 327-335.

16. Subramanian, R.. Drag on spherical particles and steady settling velocities. http://web2.clarkson.edu/projects/subramanian/ch301/notes/dragsphere.pdf
17. Haak, R, Kleinhans F, and Ochs, S (1976) The viscosity of mammalian nerve axoplasm measured by electron spin resonance. *Journal Of Physiology*. **263**, 115-137.

18. Tasaki, I., and P. M. Byrne. "Tetanic contraction of the crab nerve evoked by repetitive stimulation." *Biochemical and biophysical research communications* 106.4 (1982): 1435-1440.